Technical Report

Image Intensifier–Based Computed Tomography Volume Scanner for Angiography

Ruola Ning, PhD[1], and Robert A. Kruger, PhD[2]

Rationale and Objectives. A prototype volume computed tomography (CT) system for use in angiography was designed, constructed, and tested. The system consisted of a fixed X-ray tube, a conventional image intensifier (II) coupled to a charge-coupled device camera, and a computer-controlled turntable on which phantoms were placed. We wanted to predict, through phantom studies, the imaging performance of an II-based volume CT for direct three-dimensional (3D) reconstruction of vascular structures.

Methods. To explore the imaging performance of the system for reconstructing a vascular structure, two sets of projection images of a vascular phantom, acquired over 250 projection angles with two different-sized IIs, were digitized and used for a direct 3D cone–beam reconstruction. The signal-to-noise ratio (SNR) of each reconstructed image was measured. From these measurements, image quality was accessed as a function of the number of reconstructions averaged and the different orientations. The spatial resolution limits of the system were measured from the 3D reconstructed images of a specially designed resolution phantom for different orientations and locations.

Results. The measured SNRs of all direct 3D reconstruction images were reasonably good, and background noise levels measured from 3D reconstruction images were almost 30 Hounsfield units. The measured spatial resolution of the system was 0.5 line pairs per millimeter. However, spatial resolution was reduced around the edge of the II to nearly half that measured in the central area of the field of view.

Conclusion. An II-based volume CT scanner can produce direct 3D reconstructions of vascular structures with good image quality for intraarterial angiography.

Key Words. Computed tomography; volume computed tomography; angiography; cone–beam reconstruction.

Volume computed tomography (CT) involves using a two-dimensional (2D) area detector to acquire a set of 2D projections of a three-dimensional (3D) object and directly reconstructing the object from its 2D projections, instead of reconstructing a volume by stacking a series of 2D slice images.

Several researchers have reported on the design and performance of a variety of fluoroscopically based multiple-slice CT systems specifically designed for radiotherapy treatment planning applications and small animal and specimen research [1–10]. One application in diagnostic imaging has been proposed [11, 12]. Instead of using a conventional image intensifier (II), flat or curved fluorescent screens, coupled optically either directly to a low-light–level videocamera or indirectly to a charge-coupled device (CCD), have been studied. In both cases, imaging performance has been limited by the low detection quantum efficiency offered by these detectors compared with the relatively good detection quantum efficiency (40–50%) offered by a conventional II.

We reported the results of a computer simulation whose aim was to predict the low-contrast imaging performance capacity of a conventional X-ray II if it was incorporated

From the [1]Department of Radiology, University of Rochester Medical Center, Rochester, NY; and [2]Department of Radiology, Indiana University Medical Center, Indianapolis, IN.

This work was supported partly by National Institutes of Health grant no. 5-R01-HL31984.

Address reprint requests to R. Ning, PhD, Department of Radiology, Box 648, University of Rochester Medical Center, 601 Elmwood Ave., Rochester, NY 14642.

Received June 12, 1995, and accepted for publication after revision November 14, 1995.

Acad Radiol 1996;3:344–350
© 1996, Association of University Radiologists

Osseo 2021
U.S. Patent No. 6,381,301

into a volume CT scanner [13]. To verify the results of the computer simulation, we then constructed a prototype of a volume CT system for angiography that used an II coupled to a CCD camera as a 2D detector and presented the preliminary results from the volume CT system [14, 15]. Afterward, two volume CT systems using an II coupled to a conventional videocamera were developed: one was for excised tissue and bone [16] and the other for radiotherapy treatment planning using an II-based radiation therapy simulator [17]. The results of a volume CT system for angiography using two IIs coupled to two conventional TV cameras also have been presented [18]. The limitations in all these cases were the relatively low dynamic range, low scan stability, and nonlinearity of the conventional videocamera compared with a 2D CCD array. A II-based volume CT scanner using a time-delay integration CCD array has been developed recently for small animals and tissue samples [19]. Although this system offers high-resolution CT scans especially for the quantitative analysis of excised tissue samples in vitro, its field of view is too small and volume scanning time is inherently prohibitively long for diagnostic imaging applications.

To accurately image blood vessels in three dimensions, a sufficient number of X-ray projections of the vasculature needs to be acquired during a single intraarterial bolus injection of contrast material (<5 sec). During this time, it is impossible for conventional CT or spiral CT scanning, which uses a one-dimensional detector array, to acquire the projection data for a whole volume of interest. If the linear detector array is replaced by a 2D detector, however, sufficient data can be collected during the flow of a single bolus of contrast material to allow the reconstruction of an entire 3D volume with equal resolution in the x, y, and z directions.

In this article, we discuss our continued research with a II-based volume CT scanner for angiography, which we described previously [14, 15]. We conducted a computer simulation that was aimed at predicting the low-contrast imaging performance of which a conventional X-ray II would be capable if it were incorporated into a volume CT scanner [13]. The results of the simulation suggested that an II-based volume CT scanner is a feasible concept if the anticipated task is vascular imaging. To verify the computer simulation results, we constructed a prototype volume CT scanner that uses an X-ray II coupled to a 2D CCD camera. The device consists of a fixed X-ray tube and detector, a computer-controlled turntable on which phantoms are placed for imaging, and a computer system. In this article, we discuss the design and construction of the prototype system. We also report the results of phantom studies conducted to characterize the imaging performance of the system for direct 3D cone–beam reconstruction in terms of background noise levels, the signal-to-noise ratio (SNR) of reconstructed images, spatial resolution, and uniformity of spatial resolution, assuming that the anticipated imaging task is intraarterial angiography. We wanted to predict the imaging performance of such a volume CT device for intraarterial angiography imaging as constrained by a detector that uses an II coupled to a CCD camera. We did not attempt to correct for the geometric distortion, such as pincushion and S distortion, introduced by an II. We hypothesized that an II-based volume CT scanner would offer a 3D description of vascular structures with adequate imaging quality for intraarterial angiography.

MATERIALS AND METHODS

Prototype System

Figure 1 illustrates the diagram of the prototype system. The system was composed of a fixed X-ray tube, an aluminum filter specifically designed to reduce the dynamic range of the projection data, a computer-controlled turntable on which the phantoms were placed, an antiscatter grid, an II that has three modes (6 inch [15.24 cm], 10 inch [25.4 cm], and 14 inch [35.56 cm]), a 2D (256 × 512) VSP CCD camera (VSP Labs, Ann Arbor, MI), and a computer system.

The computer system consisted of a micro Vax II (Digital Equipment, Maynard, MA), Data Translation (Marlboro, MA) frame buffer that contained an 8-bit analog-to-digital converter (ADC) and a specially designed interface module through which the computer controlled and communicated with the X-ray generator, the stepper motor of the turntable, and the CCD camera.

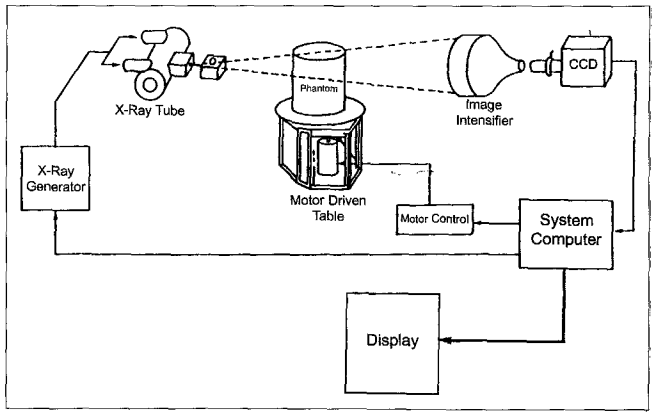

FIGURE 1. Diagram of the prototype computed tomography volume scanner. CCD = charge-coupled device.

Phantom Study

To explore the imaging performance of this system for 3D reconstructions, we imaged the vascular phantom shown in Figure 2 using two different modes of II: 10 and 14 inches. In our experiment, the diameter of the "arteries" and the postopacification iodine concentration contained in each artery are shown in Table 1.

Figure 3 is a diagram of the specially designed resolution phantom consisting of a big-body cylinder and four small identical cylinders, with each containing five sets of high-contrast wires. Each set of wires consisted of three wires with the same diameter and material. The diameter of the wires and the spacing between the wires in each set are shown in Table 2.

To measure the spatial resolution limits of the system in two different directions (vertical and horizontal) and in different locations, the four small cylinders were positioned in the big-body cylinder in locations that were determined by two coordinates (r, z), as shown in Table 3. When the resolution of the vertical planes was measured, all wires were pointed horizontally.

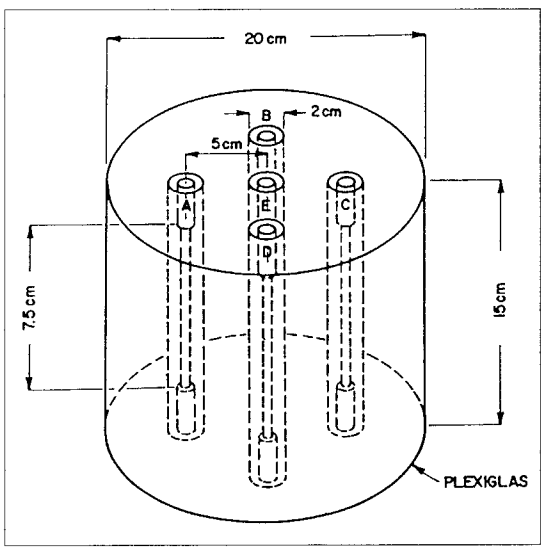

FIGURE 2. Vascular phantom.

TABLE 1: Diameter (D) of "Arteries" and Injected Iodine (I) Concentration

Vessel	D (mm)	I (mm)
A	2	50
B	2	25
C	8	50
D	8	25
E	4	50

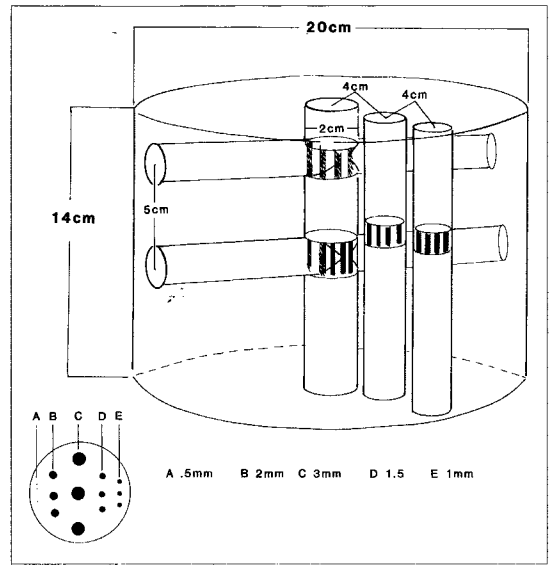

FIGURE 3. Resolution phantom.

TABLE 2: Diameter (D) of Wires and Spacing (S) Between the Wires

Vessel	D (mm)	I (mm)
A	0.5	0.5
B	2.0	2.0
C	3.0	3.0
D	1.5	1.5
E	1.0	1.0

Only set A was made from steel; the rest of the sets were made from aluminum.

TABLE 3: Positions of Four Small Cylinders

Cylinder	VR (r, z) (cm)	HR (r, z) (cm)
A	(0,0)	(0,0)
B	(5,5)	(0,5)
C	(5,0)	(5,2)
D	(8,0)	(8,2)

VR = vertical, HR = horizontal.

When the resolution of the horizontal planes needed to be measured, the wires pointed vertically.

In each case, 250 projection images, with each equally spaced over 360°, were acquired. In selecting X-ray technical factors, we chose 100 kVp for all cases. Tube current and exposure time per projection image, which varied with different phantoms and different modes of II, are shown in Table 4.

Images were digitized to 256 × 512 × 8 bits with a DT2651 frame buffer (Data Translation) and were stored on a Sun workstation (Sun Microsystems, Mountain

TABLE 4: Chosen X-Ray Technical Settings (V = 100 kVp)

II Size (inches)	Phantom	I (mA)	T (S)
10	VP	200.0	0.005
14	VP	100.0	0.005
10	RP	200.0	0.015
14	RP	200.0	0.010

II = image intensifier, I = tube current, T = exposure time vascular phantom, RP = resolution phantom.

View, CA) disk for future processing. A dark field image was subtracted from each projection to remove the direct-current offset and to correct fixed-pattern noise. To reduce the statistic fluctuation, 10 images of a dark field without a phantom were acquired and averaged before the subtraction. Prior to reconstruction, a logarithmic operation was performed on projection data with the estimated entrance beam distribution, which was obtained by acquiring and averaging 10 images of a bright field without a phantom.

Reconstruction

Our data acquisition geometry, as shown in Figure 4, was a cone–beam design. For our system setup, the cone angle was less than or equal to 10° and depended on the chosen mode of II.

Because cone–beam geometry was used, all projection data were reconstructed using Feldkamp's cone–beam algorithm [20], which is a practical 3D reconstruction algorithm. This algorithm assumes that the detector is flat. Obviously, our detector was not flat. The distortion in the reconstructions attributable to the curved input face of the image intensifier was expected.

Implementation of the algorithm was relatively straightforward. Basically, the reconstruction procedure was done in three steps: (1) weighting the projection data, (2) filtering the weighted projections with 1D ramp filter plus Hamming window, and (3) backprojecting the filtered projections. With this algorithm, a whole volume of interest could be reconstructed directly from the 2D projection data instead of stacking and reformatting the transaxial planes, as is done in conventional CT scanning.

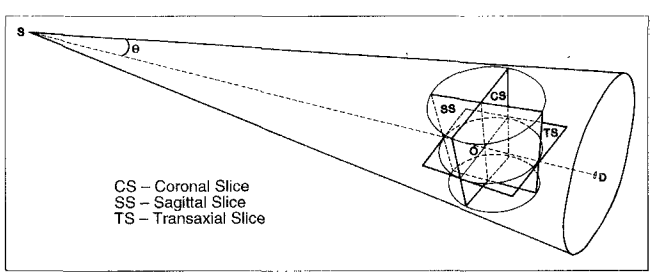

FIGURE 4. Data acquisition geometry. For our system setup, θ is less than or equal to 10°.

Here, three reconstructed images, oriented in orthogonal directions (coronal, sagittal, and transaxial), are presented. The pixel sizes of the reconstructed images were chosen so that they were compatible with the spacing between the detector cells. The size of these cells varied with the selected mode of the II and was different in the horizontal and vertical directions because of the physical size of the CCD elements. The spacing between the cells, in the horizontal and vertical directions, was measured in the object plane, which was defined as the plane perpendicular to the central X-ray beam and through the rotation center. The corresponding pixel sizes in x and y (P_{xy}) and in z (P_z) are shown in Table 5.

Once a 3D reconstruction was completed, several reconstructed adjacent slices that had the same orientation were averaged in order to increase slice thickness so that the noise level would be reduced. After reconstruction, two regions of interest were selected for signal-to-noise analysis. The first region was centered over the central arterial portion, and the second region was chosen in an adjacent region. The difference in the means of the arterial and uniform regions was taken to be equal to the signal of interest; the standard deviation in the uniform region was assumed to be representative of the local noise level. The ratio of these two values was taken to be the SNR of a reconstruction image. The SNR of each reconstructed image was measured. From these measurements, image quality and image degradation were assessed as a function of the number of reconstructions averaged and the different orientations.

RESULTS

To know the effects of the variations in slice thickness, several adjacent reconstructed slices were averaged. Averaging one, two, four, and eight adjacent slices had

TABLE 5: Sizes of Detector Elements and Pixel Sizes of Reconstructions

II Size (inches)	SH (mm)	SV (mm)	P_{xy} (mm)	P_z (mm)
10	0.35	0.50	0.4	0.50
14	0.50	0.75	0.5	0.75

II = image intensifier, SH = horizontal spacing, SV = vertical spacing, P = pixel size.

two effects. First, the slice thickness was increased in proportion to the number of averaged slices. Second, the resultant noise levels in the averaged reconstructed images were expected to decrease inversely with the square root of the number of averaged slices, *n*. Figure 5 shows the effect of slice averaging on the noise level of the reconstructed images. As can be seen in Figure 5, the expected increase in SNR was obtained when the adjacent slices were averaged.

Figure 6 shows four reconstruction images of the vascular phantom, which were averaged to 2 mm thick. They all were reconstructed from 250 nonsubtraction projections using Feldkamp's algorithm. From the images, one can see that vessel B, which was originally 2 mm in diameter and was opacified by 25 mg/ml of iodine concentration, is well defined in all the images in which it is contained. Comparing the images resulting from the 10-inch II with the image from the 14-inch II, it can be seen that the size of the reconstructed vessels are different, suggesting that with different sizes of II, II-based volume CT can have a different resolution. The measured SNRs for vessels B and E with a 10-inch II in three different planes—transverse, coronal, and sagittal—are shown in Table 6. The results display a nearly uniform measured SNR for the same vessel in different orientations, and the measured background noise level is approximately 30 Hounsfield units (H).

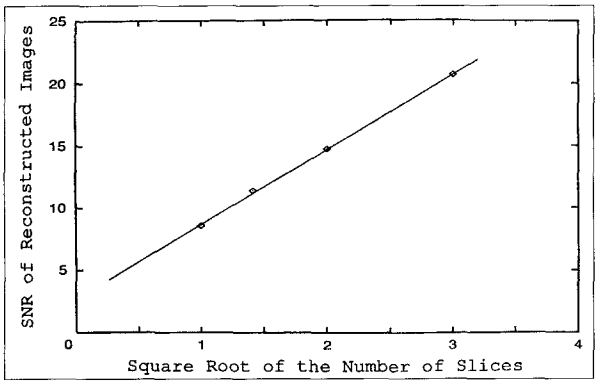

FIGURE 5. Measured signal-to-noise ratio of reconstructed images as a function of the square root of the number of averaged slices, *n*.

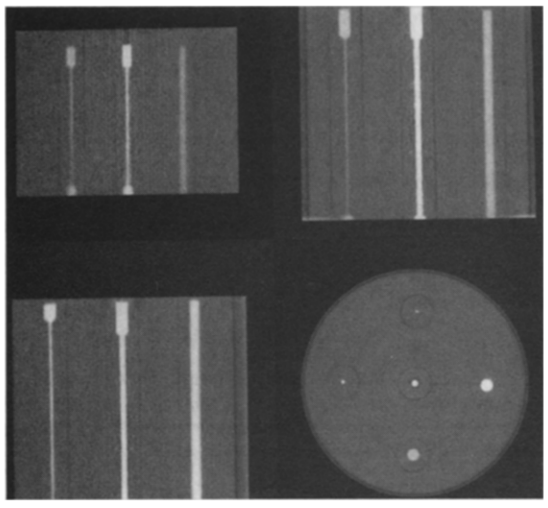

FIGURE 6. The images were reconstructed from the 250 projections of the vascular phantom, which were averaged to 2 mm thick. The upper left image is a sagittal slice with a 14-inch image intensifier (II) as the detector. The upper right is a sagittal plane with a 10-inch II. The lower left is a coronal cut with a 10-inch II. The bottom right is a transaxial slice with a 10-inch II.

To measure the spatial resolution of the prototype volume CT system, we reconstructed eight images of the resolution phantom from 250 projections using Feldkamp's algorithm. The resultant images are shown in Figures 7 and 8. These images were single slices done without slice averaging. In both figures, the top left image is a sagittal reconstruction that shows how the four small resolution cylinders were arranged. In Figure 7, the remaining three images are transaxial reconstructions at different levels in the vertical direction, *z*. These three images were used to measure the spatial resolution of the system horizontally. The following can be observed from these three images: The 0.5-mm steel wires cannot be resolved in any image, and the 1.0-mm aluminum wires can be resolved around the center of the II but cannot be resolved around the periphery of the II. In Figure 8, the remaining three images are the coronal reconstructions at different depths; these were used to measure the spatial resolution of the system vertically. The same results as in Figure 7 can be seen from these three images. This means that at best, the spatial resolution of the system is 0.5 line pairs per millimeter (lp/mm) and that the spatial resolution of the prototype volume CT is not uniform from the center of the II to its edge.

TABLE 6: The Measured SNR for Vessel B and E

Vessel	Orientation	Background Noise Level (H)	SNR
B	TP	31	18.5
B	CP	30	40.1
B	SP	31	19.2
E	TP	30	42.0
E	CP	30	41.1
E	SP	31	40.7

SNR = signal-to-noise ratio, H = Hounsfield unit, TP = transverse plane, CP = coronal plane, SP = sagittal plane.

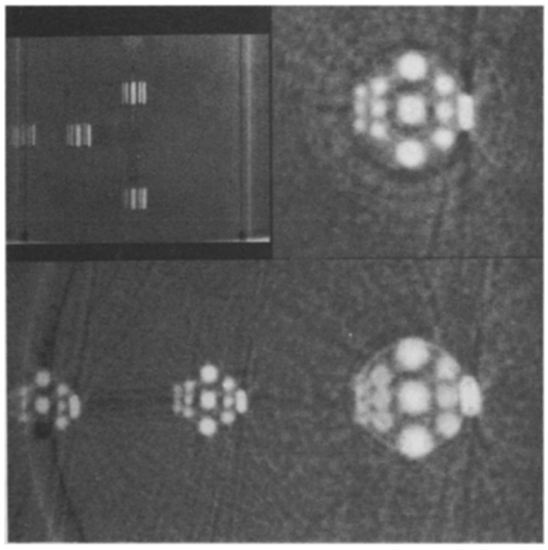

FIGURE 7. The images were reconstructed from the 250 projections of the resolution phantom with a 10-inch image intensifier (II), which are single slices done without slice averaging. These images were used to measure the resolution in horizontal planes. The top left image is a sagittal cut, which shows how the four small resolution cylinders were arranged. The remaining three images are the transaxial slices at different levels. From these images, it can be seen that 1.0-mm wires can be resolved by the system and that the resolution is not uniform from the center to the edge of the II.

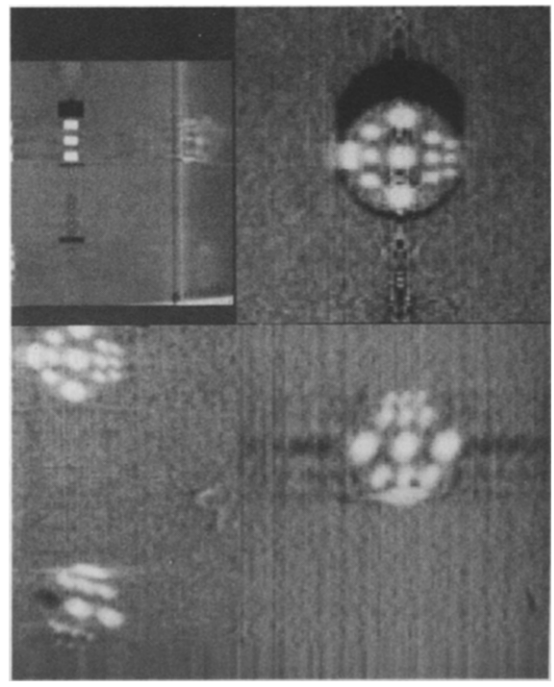

FIGURE 8. The images were reconstructed from the 250 projections of the resolution phantom with a 10-inch image intensifier (II), which are single slices done without slice averaging. These images were used to measure the resolution in vertical planes. The top left image is a sagittal cut, which shows how the four small resolution cylinders were arranged. The remaining three images are the coronal slices at different depths. From these images, it can be seen that 1.0-mm wires can be resolved by the system and that the resolution is not uniform from the center to the edge of the II.

DISCUSSION

Direct 3D reconstructed images of the vascular phantom from 250 nonsubtraction projections were obtained using the prototype volume CT system. In the reconstructed images, all reconstructed "arteries" of the vascular phantom were well defined, and the measured SNRs of all the reconstructions were good. The measured background noise level was approximately 30 H. Note that the lowest iodine concentration injected into the arteries was 25 mg/ml, which is 3–13 times lower than that currently used in standard intraarterial angiography. Our results show that by using the II-based volume CT scanner, direct 3D reconstructions of the vascular structures could be obtained with a good SNR for intraarterial angiographic applications from 250 projections.

We used slice averaging to reduce the noise level in a reconstructed image. The result followed the expected $\sqrt{n}$ behavior, where n is the number of averaged slices. Thus, in practice, the noise level in a 3D reconstructed image can be reduced by averaging several adjacent slices in the same orientation, with an attendant increase in slice thickness.

The spatial resolution of the prototype volume CT system was estimated by evaluating the direct 3D reconstruction images of the specially designed resolution phantom. The resolution of the system measured with a high-contrast wire pattern was 0.5 lp/mm for a 10-inch II in the horizontal and vertical directions around the central part of the II. This value is close to the resolution of the detector, which is the II coupled to the CCD camera. This result suggests that the resolution of the II-based volume CT is limited by the number of TV lines of the CCD camera. The measured spatial resolution value of the system was the same as the interslice resolution (x–y plane) in conventional CT scanning. However, in a direction orthogonal to the slice plane (z direction), the resolution of the volume CT system was at least three times better than that of the conventional CT scanner when a volume was formed by stacking a series of slices in the conventional CT scanner. From these results, we conclude that the direct 3D reconstruction images obtained with the II-based volume CT will have equal resolution in the x and y directions and that they will be superior to conventional CT scanning in the resolution of the z direction.

The resulting images from the projection data of the resolution phantom also show that around the periphery of the II, the resolution of the system was reduced

to 0.25 lp/mm for the 10-inch II. This resolution loss might have been due primarily to the pincushion distortion of the II. To achieve a uniform spatial resolution from the center to the edge of the field of view, the pincushion distortion may need to be corrected.

Overall, a background noise level of approximately 30 H can be expected using our system: an II, an 8-bit ADC, and a CCD camera with about a 1000:1 dynamic range. Although the background noise levels resulting from our prototype system were almost 10 times greater than what is currently encountered with a conventional CT scanner, such noise performance should be more than adequate for performing intraarterial angiography. The iodine concentration levels expected from standard intraarterial angiography procedures range from 100 mg/ml with aortic injections to as much as 370 mg/ml for selective injections.

The iodine concentration of 100 mg/ml would be expected to provide about 2,500 H of imaging contrast, more than enough to compete with the anticipated imaging noise. With a data acquisition rate of 60–120 frames/sec (512 × 512 × 8 bit), 250 views can be acquired within 2.1–4.2 sec and direct 3D reconstruction of vascular structure from 250 2D projections can be obtained with 0.5 lp/mm spatial resolution along the x, y, and z directions.

The background noise level obtained from the prototype is consistent with what was predicted in our computer simulation when an 8-bit ADC and a 1,000:1 dynamic range of a CCD were used, but it was two times higher than what was predicted in our simulation, in which a 12-bit ADC and 4,000:1 dynamic range of a CCD camera were used [13]. This implies that there is some latitude to further improve the low-contrast imaging performance of the system by upgrading the system with a 12-bit ADC and a CCD camera that has a 4,000:1 dynamic range.

In summary, it appears that an II-based CT system can produce a direct 3D reconstruction of vascular structures with good image quality if the anticipated imaging task is intraarterial angiography. Questions still remain about the geometry distortion introduced by an II and whether this system can be used for intravenous angiography, in which the iodine concentration levels can be as low as 6 mg/ml, and still provide about 100 H of imaging contrast. Both these questions are being addressed in our current research efforts. In addition, because this table-top prototype is not suitable for animal and patient studies, a volume CT system based on a conventional CT gantry is being assembled to verify the results from our phantom studies and perform animal studies.

ACKNOWLEDGMENTS

We thank Thomas Morris and Alyce Norder for their assistance in revising this article.

REFERENCES

1. Baily NA, Keller RA, Jakowatz CV, Kak AC. The capability of fluoroscopic systems for the production of computerized axial tomograms. *Invest Radiol* **1976**;11:434–439.
2. Oldendorf WH. Some possible applications of computerized tomography in pathology. *J Comput Assist Tomogr* **1980**;4:141–144.
3. Duinker S, Geluk RJ, Mulder H. Transaxial analogue tomography. *Oldeft Sci Eng* **1978**;1:448–453.
4. Harrison RM, Farmer FT. The determination of anatomical cross sections using a radiotherapy simulator. *Br J Radiol* **1978**;59:41–66.
5. Sequin FH, Burstein P, Bjorkholm PJ, Homburger F, Adams RA. X-ray computed tomography with 50-μm resolution. *Appl Optics* **1985**;24:4117–4123.
6. Kotre CJ, Harrison RM, Ross WM. A simulator-based CT system for radiotherapy treatment planning. *Br J Radiol* **1984**;57:631–635.
7. Redpath AT, Wright DH. The use of a simulator and treatment planning computer as a CT scanner for radiotherapy planning. In: *Proceedings of the International Conference on the Use of Computers in Radiotherapy.*, **1984**:281–287.
8. Qu LZ, Nalcioglu Q, Roeck W, Rabani B, Colman M. *Video based X-ray computed tomography* (monograph no. UCI/DPE/85-05). Irvine: University of California, Department of Radiological Science, **1985**.
9. Boone JM, Alexander GM, Seibert JA. Personal computer fluoroscopy CT system for small animal and specimen research. *Radiology* **1990**;177:136.
10. Morton EJ, Webb S, Bateman JE, Clarke LJ, Shelton CG. Three-dimensional X-ray microtomography for medical and biological applications. *Phys Med Biol* **1990**;35;805–820.
11. Ritman EL, Jorgensen SM, Rhyner MH, Roessler RW, Whitlock SV, Caskey PE. *Computer assisted radiology.* In: Lemke H, Rhodes LM, Jaffee CC, Felix R, eds. *X-ray image train for a computed tomography approach to intravenous coronary arteriography.* Berlin, Germany: Springer-Verlag,**1985**:65–69.
12. Ritman EL, Robb RA, Harris LD. *Imaging physiological functions: experience with the DSR.* Philadelphia: Praeger, **1985**:302.
13. Ning R, Kruger RA. Computer simulation of imaging intensifier-based CT detector: vascular application. *Med Phys* **1988**;15:188–192.
14. Ning R, Hu H, Kruger RA. Image intensifier-based CT volume imager for angiography. *SPIE* **1988**;914:282–287.
15. Ning R, Kruger RA, Hu H. Image intensifier-based CT volume imager for angiography: system evaluation. *SPIE* **1989**;1090:131.
16. Feldkamp LE, Goldstein SA, Parfitt AM, Jesion G, Kleerekoper M. The direct examination of three-dimensional bone architecture in vitro by computed tomography. *J Bone Miner Res* **1989**;4:3–11.
17. Silver MD, Yahata M, Saito Y, Siversetal EA. Volume CT of anthropomorphic phantoms using a radiation therapy simulator. *SPIE* **1992**;1651:197.
18. Saint-Felix D, Campagnelo R, Rolland Y, et al. 3D computerized X-ray angiography: first in vivo results. *Radiology* **1992**;185:304.
19. Holdworth DW, Drangova M, Fenster A. A high-resolution XRII-based quantitative volume CT scanner. *Med Phys* **1993**;20:449.
20. Feldkamp LA, Davis LC, Kress JW. Practical cone-beam algorithm. *J Opt Soc Am A* **1984**;1:612–619.